ЦРНОГОРСКА АКАДЕМИЈА НАУКА И УМЈЕТНОСТИ
ГЛАСНИК ОДЈЕЉЕЊА ПРИРОДНИХ НАУКА, 25, 2022.

ЧЕРНОГОРСКАЯ АКАДЕМИЯ НАУК И ИСКУССТВ
ГЛАСНИК ОТДЕЛЕНИЯ ЕСТЕСТВЕННЫХ НАУК, 25, 2022

THE MONTENEGRIN ACADEMY OF SCIENCES AND ARTS
PROCEEDINGS OF THE SECTION OF NATURAL SCIENCES, 25, 2022

UDK 539.319
UDK 532.5:612.219

Marko V. Lubarda,* *Vlado A. Lubarda*†

ON THE MOTION OF AN EVAPORATING RESPIRATORY DROPLET

A b s t r a c t

An analysis of the projectile motion in stagnant air is presented for an evaporating respiratory micro-droplet which has been ejected from the mouth as an isolated droplet. It is assumed that the air resistance is a nonlinear function of the droplet's velocity and that the rate of decrease of the droplet's external surface area depends only on the relative humidity and the ambient temperature. The droplet's initial content is considered to be 98 wt% water, 1 wt% salt and 1 wt% protein. The change of the average density of the droplet due to water evaporation is determined, up to the instant when the droplet reduces to its nucleus, consisting of salt and dry protein only. The numerical solution of the governing differential equations of droplet's motion gives the trajectories of different-sized droplets ejected at different velocities and angles, and under different relative humidities and rates of evaporation. The evaporation times are compared with the times for droplets to reach the ground after being ejected from a given height. The maximum horizontal and vertical distances reached by the droplet are evaluated in the presence of wind and discussed in the context of possible infection spreading.

Keywords: density; drag force; droplet nucleus; evaporation rate; relative humidity; respiratory droplet; SARS-CoV-2, wind effect

1 Introduction

There has been a large amount of research devoted to biophysical and chemical aspects of the investigation of infection spreading by inhalation of airborne droplets containing bacteria or viruses, which has recently intensified due to the pandemic caused by SARS-Cov-2 (Stadnytskyi et al., 2020;

*M.V. Lubarda, Department of Mechanical and Aerospace Engineering, University of California, San Diego; Member of the Center for Young Scientists and Artists, Montenegrin Academy of Sciences and Arts (mlubarda@ucsd.edu).

†V.A. Lubarda, NanoEngineering Department, University of California, San Diego; Member of the Montenegrin Academy of Sciences and Arts (vlubarda@ucsd.edu).

Balachandar et al., 2020; Jayaweera et al., 2020; Lieber et al., 2021). Normal speaking and expiratory activities can emit thousands of respiratory droplets per second. The volume and droplet count increase with loudness; loud speaking and coughing emit even more droplets. According to early measurements by Duguid (1946), 95% of the emitted respiratory droplets had the diameter between 2 and 100 μm, the most common diameter being between 4 and 8 μm. Similar size distributions were found in droplets produced by sneezing, coughing, and normal speaking; the smaller droplets were relatively more numerous in the case of sneezing. More recent measurements with sub-micron resolution indicate that 80–90% of particles produced by human expiratory activities are smaller than 1 μm (Papineni and Rosenthal, 1997). The measured size, however, could correspond to the size of the dry droplet residue (Morawska et al., 2009), because the time spent in the air before the droplet's detection and its size measurement could have been long enough for significant evaporation to take place; see also Xie et al. (2009) and Tellier et al. (2019). The fractional viral load of respiratory droplets, i.e., the average number of virions per droplet, has been discussed by Mittal et al. (2020). The motion of respiratory droplets can also be affected by their interaction with other particles of non-biological origin present in the air (Morawska et al., 2006).

Small droplets (say less than 10 μm initial diameter, further decreasing in size due to evaporation) are easily carried by a puff of exhaled air produced by breathing, talking, coughing, or sneezing, with small relative velocity, and can remain afloat for a long time; they can be further convected by outside wind or indoor draft or ventilation (Liu and Novoselac, 2014, Li et al., 2018; Wang et al., 2019; Anchordoqui and Chudnovsky, 2020; Cheng et al., 2020). As a result, the probability of their inhalation and thus infection, if they contain viruses such as SARS-CoV-2, substantially increases. The Brownian motion of very small (aerosol) droplets has also been studied using the Langevin differential equation with a stochastic term due to random interactions of the droplet with the individual molecules of the air (Das et al., 2020). On the other hand, large droplets (say, greater than 50 or 100 μm-diameter), if ejected from the mouth into the air outside of the exhaled puff, move like projectiles. These droplets are rapidly slowed down by drag resistance from the ambient air, and fall to the ground or nearby surfaces or people, which presents a risk of infection when such droplets are touched and transmitted to mouth or eyes. If large droplets are ejected within the exhaled jet stream, they initially move within the advancing and slowing puff, but can quickly exit from it due to their large weight and developed velocity relative to the puff (Xie et al., 2007; Wang et al., 2020). Once outside the puff, these droplets move as isolated projectiles with initial positions and speeds determined from the more involved analysis describing their motion within the moving and expanding puff, and corresponding to the instant when they exit the puff. Larger droplets may also be potentially more infectious due to higher viral content (Li et al., 2021). The trajectories of intermediate-size droplets are more complex as they move within the puff longer distances and may evaporate to their nucleus size while still within the puff (Balachandar et al., 2020; Bourouiba, 2020; Giovanni, 2020; Vuorinen et al., 2020).

In this paper, we present an analysis of the projectile motion of an isolated micro-droplet ejected from the mouth at different angles and initial velocities. The air resistance is represented by a nonlinear function of the droplet's velocity, and the rate of decrease of the droplet's external surface area is assumed to depend only on the relative humidity and the ambient temperature. The droplet's initial content is considered to be 98 wt% water, 1 wt% salt (NaCl), and 1 wt% protein (mucus). The change of the average density of the droplet caused by water evaporation is determined, up to the instant when all water evaporates and the droplet reduces to its nucleus (droplet residue), consisting of salt and dry protein only. This also specifies the change of the droplet's mass, which enables numerical solution of the governing differential equations of the droplet's motion, for an arbitrary angle of ejection and initial velocity, corresponding to either soft or loud speaking, coughing, or sneezing. The trajectories of different-sized droplets are determined under different relative humidities. In each case the maximum horizontal distance traveled by the droplet in stagnant air is rapidly reached, which is followed by an essentially vertical descent of the droplet. The maximum

horizontal reach in soft talking is compared to that in coughing. We also evaluate and compare the time for the droplet to evaporate down to its nucleus size and the time for the droplet to reach the ground when ejected from a given height. The effects of the angle of ejection of the droplet on its maximum horizontal and vertical reach and the entire trajectory are discussed. The wind effects are also included in the analysis and discussed in the context of infection spreading by transmission of viruses and other pathogens via respiratory droplets.

2 Projectile motion of an evaporating droplet with a nonlinear drag force

For smaller droplets and for sufficiently small initial velocities, the Reynolds number of an isolated droplet is below 1 and the linear Stokes' type drag model can be adopted in the study of such droplet's motion. For larger droplets (say, greater than about 5 microns) and for larger initial velocities (e.g., velocities about 10 m/s as during coughing, or up to 50 m/s as during sneezing), the Reynolds number, at least in the early stage of the droplet's motion, is in the range $1<\mathrm{Re}<1000$, and the drag force becomes a nonlinear function of velocity. To encompass the entire range of Reynolds number, the drag force in still air is commonly written as

$$\mathbf{F}_{\mathrm{d}} = -\frac{1}{2}\,\rho_{\mathrm{air}} A c_{\mathrm{d}} v \mathbf{v}\,, \quad A = \pi R^2\,, \tag{2.1}$$

where the drag coefficient c_{d} depends on the Reynolds number, in accord to experimental data (Schlichting, 1979; White, 2006). The air density is ρ_{air}, the current radius of the droplet is R, its velocity vector is $\mathbf{v}$, and v is its magnitude. The following expression fits this data sufficiently well in the range $0.2 < \mathrm{Re} \le 3\times 10^5$ (Lapple, 1951; Khan and Richardson, 1987)

$$c_{\mathrm{d}} = \begin{cases} 24\mathrm{Re}^{-1} + 3\mathrm{Re}^{-0.28}, & 0.2 \le \mathrm{Re} \le 10^3\,, \\ 0.458\,, & 10^3 \le \mathrm{Re} \le 3\times 10^5\,. \end{cases} \tag{2.2}$$

Below $\mathrm{Re} = 0.2$, the dominant contribution to c_{d} is $24/\mathrm{Re}$, which gives rise to linear drag force, proportional to velocity (Stokes' flow). Other fitting expressions have also been proposed and used, e.g., Zhu et al. (2006), Xie et al. (2007), Wang et al. (2020), Cheng et al. (2020), and Lieber et al. (2021). For example, Xie et al. (2007), used $c_{\mathrm{d}} = 24\mathrm{Re}^{-1} + 4\mathrm{Re}^{-1/3}$ for $\mathrm{Re} \le 1000$ and $c_{\mathrm{d}} = 0.424$ for $\mathrm{Re} \ge 1000$. The Reynolds number at an arbitrary time t during the motion of an evaporating droplet is defined by

$$\mathrm{Re}(t) = \frac{2R(t)v(t)}{\nu_{\mathrm{air}}}\,. \tag{2.3}$$

The kinematic viscosity of air is $\nu_{\mathrm{air}} = \eta_{\mathrm{air}}/\rho_{\mathrm{air}}$, where η_{air} is its dynamic viscosity. Typically, the Reynolds number of a relatively large droplet is below 1,000; for example, for $\nu_{\mathrm{air}} = 1.516\times$

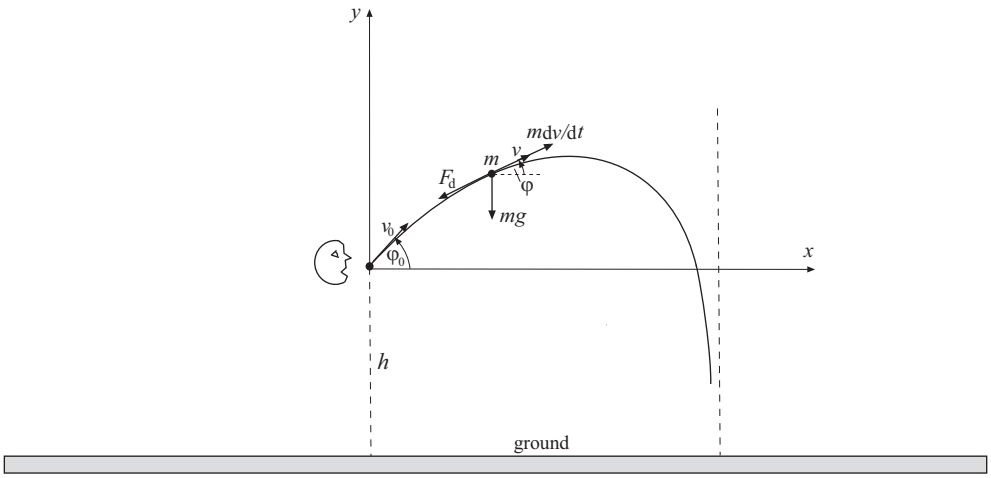

Figure 1: The motion of a droplet of initial mass m_0 ejected at height h above the ground with initial velocity v_0 at an angle φ_0 with respect to the horizontal x axis. In the position shown at time t, the forces acting on the droplet are its weight mg and the drag force $F_{\rm d}$, opposite to its current velocity v. The horizontal and vertical components of velocity are $v_x = v\cos\varphi$ and $v_y = v\sin\varphi$.

$10^{-5}\,{\rm m}^2/s$ and at the instant when $v = 10$ m/s and $R = 100\,\mu$m, the Reynolds number is ${\rm Re} \approx 132$. On the other hand, for a small droplet of radius $R = 5\,\mu$m and current velocity $v = 1$ m/s, the Reynolds number is ${\rm Re} \approx 0.66$. If the air surrounding a droplet moves with the velocity $v_{\rm a}$, the relative velocity $v - v_{\rm a}$ should be used in place of the total velocity in the expression for the drag force (2.1) and the definition of the Reynolds number (2.3).

Suppose that a droplet having initial mass m_0 and corresponding initial radius R_0 is emitted from the mouth at height h above the ground with initial velocity v_0 at an angle φ_0 relative to the horizontal x direction (Fig. 1). At an arbitrary time t during its projectile-type motion, the mass of the droplet is $m < m_0$, its radius $R < R_0$, and its velocity $v < v_0$. The current inclination angle of the velocity vector is φ. The vectorial form of the differential equation of the droplet's motion in still air is then

$$m\,\frac{{\rm d}\mathbf{v}}{{\rm d}t} = \mathbf{F}_{\rm d} + m\mathbf{g} - \mathbf{u}_{\rm rel}\,\frac{{\rm d}m}{{\rm d}t}\,. \tag{2.4}$$

The average ejection velocity, relative to the droplet, of all particles leaving the droplet due to evaporation is $\mathbf{u}_{\rm rel} = \mathbf{u} - \mathbf{v}$, and $\mathbf{g} = \{0, -g\}$ is the gravitational acceleration. The buoyancy force is ignored as the density of a respiratory droplet is about 1000 times greater than the density of the air. By assuming that $\mathbf{u}_{\rm rel} = 0$, the governing differential equations for the velocity components (v_x, v_y) of the droplet are

$$m\,\frac{{\rm d}v_x}{{\rm d}t} = -F_{\rm d}\,\frac{v_x}{v}\,, \quad m\,\frac{{\rm d}v_y}{{\rm d}t} = -F_{\rm d}\,\frac{v_y}{v} - mg\,, \tag{2.5}$$

where $F_{\rm d} = \rho_{\rm air} A c_{\rm d} v^2/2$ from (2.1). Upon substitution of the latter expression for $F_{\rm d}$ into (2.5) and division by the current mass $m = \rho V$, where ρ is the (average) mass density of the droplet at time t and $V = 4\pi R^3/3$ is the droplet's current volume, we get

$$\frac{{\rm d}v_x}{{\rm d}t} = -\frac{3\rho_{\rm air}}{8\rho}\,\frac{c_{\rm d}}{R}\,v_x v\,, \quad \frac{{\rm d}v_y}{{\rm d}t} = -\frac{3\rho_{\rm air}}{8\rho}\,\frac{c_{\rm d}}{R}\,v_y v - g\,, \tag{2.6}$$

with the drag coefficient $c_{\rm d}$ defined by (2.2). The accompanying initial conditions are $v_x(0) = v_0 \cos\varphi_0$ and $v_y(0) = v_0 \sin\varphi_0$.

Equations (2.6) are two coupled differential equations, which require numerical integration, provided that the expressions for $R = R(t)$ and $\rho = \rho(t)$ are determined, corresponding to the rate by which the mass of the droplet evaporates, as elaborated upon in section 3. After the velocity components v_x and v_y have been determined, the (x, y) coordinates of the trajectory of the droplet follow by numerical quadrature from $x(t) = \int_0^t v_x(\theta)\,{\rm d}\theta$ and $y(t) = \int_0^t v_y(\theta)\,{\rm d}\theta$, as reported in section 4.

2.1 Motion of the droplet's residue

At some instant of motion (t_*), all water from a respiratory droplet evaporates and the droplet is reduced to its nucleus (salt and dry protein residue) of a radius denoted by R_*. From that instant on, i.e., for time $t \geq t_*$, the motion of this non-volatile residue proceeds as the motion of a non-evaporating spherical particle of constant radius R_*. The initial conditions for this motion are $v_x(t = t_*) = v_* \cos\varphi_*$, $v_y(t = t_*) = v_* \sin\varphi_*$, and $x(t = t_*) = x_*$, $y(t = t_*) = y_*$. The quantities $(t_*, v_*, \varphi_*, x_*, y_*)$ have been determined from the preceding analysis of the motion of the evaporating droplet, and correspond to the end of that part of motion, i.e., the instant when the droplet evaporates to its nucleus size of radius R_*. The numerical analysis of the motion of the evaporating droplet shows that the Reynolds number rapidly diminishes with time, after the droplet's emission from the mouth, because the droplet's velocity rapidly diminishes, as well as its radius. As a consequence, the motion of the droplet's residue is in many cases the motion under linear (Stokes') drag force, $F_{\rm d} = cv$, where $c = 6\pi\eta_{\rm air}R_*$. It then readily follows that the velocity components of the droplet's residue are

$$\begin{aligned} v_x(t) &= v_* \cos\varphi_*\, e^{-k_*(t-t_*)}\,, \quad k_* = \frac{c}{m_*}\,, \quad t \geq t_*\,, \\ v_y(t) &= (v_{\rm t} + v_* \sin\varphi_*)\, e^{-k_*(t-t_*)} - v_{\rm t}\,, \quad v_{\rm t} = \frac{g}{k_*}\,, \end{aligned} \tag{2.7}$$

where $m_* = \rho_* V_*$ is the mass of the droplet's residue and $V_* = 4\pi R_*^3/3$ is its volume. The velocity $v_{\rm t}$ is the so-called terminal velocity, at which the drag force balances the gravity force ($cv_{\rm t} = m_* g$). The corresponding coordinates of the droplet's residue are given by

$$\begin{aligned} x(t) - x_* &= \frac{1}{k_*}\, v_* \cos\varphi_* \left[1 - e^{-k_*(t-t_*)}\right], \quad t \geq t_*\,, \\ y(t) - y_* &= \frac{1}{k_*}\,(v_{\rm t} + v_* \sin\varphi_*) \left[1 - e^{-k_*(t-t_*)}\right] - v_{\rm t}(t - t_*). \end{aligned} \tag{2.8}$$

By eliminating $t - t_*$ in (2.8), the $y = y(x)$ representation of the residue trajectory can also be explicitly given. For sufficiently large times ($t \gg t_*$), the residue approaches the vertical asymptote $x = x_* + (v_*/k_*)\cos\varphi_*$, with the residue's time-dependent position y being given by

$$y(t) = y_* + \frac{1}{k_*}\,(v_{\rm t} + v_* \sin\varphi_*) - v_{\rm t}(t - t_*)\,. \tag{2.9}$$

3 Evaporation of a droplet

Suppose that a respiratory droplet is exhaled from mouth as a spherical particle of initial radius R_0 and corresponding mass m_0. It will be assumed that 98% of m_0 is pure water ($m_{\rm w}^0 = 0.98 m_0$), 1% a salt (NaCl), and 1% a protein (mucin), i.e.,

$$m_0 = m_{\rm w}^0 + m_{\rm s} + m_{\rm p} = m_{\rm w}^0 + f_{\rm s} m_0 + f_{\rm p} m_0\,, \quad (f_{\rm s} = 0.01\,,\ f_{\rm p} = 0.01)\,. \tag{3.1}$$

This initial content of the respiratory saliva droplet is taken somewhat arbitrarily, from a large variety of data found in the literature (Sarkar et al. 2019; Chaudhuri et al., 2020; Netz, 2020; Stadnytskyi, 2020; Lieber, 2021), but the analysis proceeds similarly if the initial droplet's content is assumed differently, which mainly affects the size of the droplet's residue. Furthermore, we assume that the salt and protein are non-volatile at common ambient temperatures ($m_{\rm s}=$ const. and $m_{\rm p}=$ const.), and that only water evaporates during the droplet's motion, i.e., the time rate of change of the droplet's mass is equal to the time rate of change of the water content in the droplet ($\mathrm{d}m/\mathrm{d}t=\mathrm{d}m_{\rm w}/\mathrm{d}t$). Initially, the water and salt in an exhaled droplet form an aqueous solution of mass $m^0_{\rm sol}=m^0_{\rm w}+m_{\rm s}=m_0-m_{\rm p}$ in which Na^+ and Cl^- ions are dispersed throughout the water, with the initial mass (weight) concentration of salt

$$\frac{m_{\rm s}}{m^0_{\rm sol}}=\frac{m_{\rm s}}{m_0-m_{\rm p}}=\frac{f_{\rm s}}{1-f_{\rm p}}\,. \tag{3.2}$$

The objective is to determine the time-dependent decrease of the mass and density of the droplet during its evaporation.

The evaporation of a droplet is a complicated physical and chemical process that can be analyzed with various degrees of complexity and sophistication. This may include the consideration of the energy equation and the heat and mass transfer between the droplet and its surroundings, and the effects of the ambient temperature and the temperature of the droplet on its evaporation rate (e.g., Kukkonen et al, 1989; Sun and Ji, 2007; Liu et al., 2019; Chaudhuri et al., 2020; Chen, 2020; Netz; 2020). In our present analysis, we adopt a simplified phenomenological approach in which it is assumed that during evaporation the time rate of change of the external surface of the droplet, $S(t)=4\pi R^2(t)$, is a given constant (s), dependent only on the relative humidity (RH) and the ambient temperature ($T_{\rm amb}$). Such an assumption is reasonable because the evaporation is driven by the difference between the concentration of the water vapor at the surface of the droplet and in the surrounding air. Thus, we write

$$\frac{\mathrm{d}S}{\mathrm{d}t}=-s\,,\quad s=s(\mathrm{RH},T_{\rm amb})\,. \tag{3.3}$$

A possible effect of the velocity of the moving droplet on its evaporation rate s is not included in (3.3). A surface evolution expression of the type (3.3) has also been adopted in the early work by Wells (1934), and in the later work by Kayser and Bennett (1977). Alternative expressions could also be adopted, such as $\mathrm{d}m/\mathrm{d}t=-\kappa$ and $\mathrm{d}m/\mathrm{d}t=-\mu S$, where κ and μ depend on the ambient and droplet's temperatures and other physical parameters of the evaporation process. The former expression was derived by Kukkonen et al. (1989) and later used by Cheng et al. (2020).

Returning to the rate expression (3.3), to determine the dependence of s on RH at a given temperature $T_{\rm amb}$, we use the results from the analysis of evaporation kinetics of water droplets by Su et al. (2018). From their Fig. 5, the initial radius of a spherical droplet $R_0=25\,\mu$m is reduced by evaporation to the radius $R=5\,\mu$m in approximately 2.2 seconds for RH=0%, 2.75 seconds for RH=20%, 4.5 seconds for RH=50%, 11.5 seconds for RH=80%, and in about 23 seconds for RH=90%. The ambient temperature was $T_{\rm amb}=293$ K. By using this, from (3.3) it follows that the corresponding values of s are $\{3.427, 2.742, 1.676, 0.656, 0.328\}\times 10^{-9}\,\mathrm{m}^2/\mathrm{s}$. These values are well-interpolated by a linear fit $s=s_0(1-\mathrm{RH}/100)$, where $s_0=3.427\times 10^{-9}\,\mathrm{m}^2/\mathrm{s}$. Since saliva droplets evaporate a little slower than pure water droplets, the value of s_0 can be taken a little lower, and we adopt the following expression

$$s=s_0(1-\mathrm{RH}/100)\,,\quad s_0=3.25\times 10^{-9}\,\mathrm{m}^2/\mathrm{s}\,. \tag{3.4}$$

For other than room ambient temperatures, the expression (3.4) may still approximately apply by adjusting the value of the temperature-dependent coefficient $s_0=s_0(T_{\rm amb})$. Because the evapora-

tion is more rapid at higher ambient temperature, the coefficient s_0 is expected to be a monotonically increasing function of T_{amb}.

By integrating (3.3), it follows that

$$S(t) = S_0\left(1 - \frac{t}{\tau}\right), \quad R(t) = R_0\left(1 - \frac{t}{\tau}\right)^{1/2}, \quad \tau = \frac{S_0}{s}, \quad S_0 = 4\pi R_0^2 . \tag{3.5}$$

These expressions apply until all the water evaporates and the droplet's radius reduces to the radius of the droplet's nucleus. The square-root dependence of R on time t in (3.5) can be compared with the well-known radius-square relation between the initial and the current radius of the droplet, $R^2 - R_0^2 = kt$ ($k = \mathrm{const.}$); see Jakubczyk (2012), Netz (2020), and Balachandar et al. (2020).

Salt is soluble in water up to its weight concentration of 0.357. In this range of concentration the experimental data on the density of the aqueous solution of NaCl is well reproduced by a linear fit

$$\rho_{\mathrm{sol}}^{\mathrm{aq}} = \rho_{\mathrm{w}} + \kappa\,\frac{m_{\mathrm{s}}}{m_{\mathrm{sol}}^{\mathrm{aq}}}, \quad 0 \le \frac{m_{\mathrm{s}}}{m_{\mathrm{sol}}^{\mathrm{aq}}} \le 0.357 , \tag{3.6}$$

where $\rho_{\mathrm{w}} = 997\,\mathrm{kg/m^3}$ is the mass density of water at room temperature, and $\kappa = 755\,\mathrm{kg/m^3}$ is the slope of this linear fit. As the water evaporates from a droplet, the salt concentration increases, and after it reaches the saturation concentration of 0.357, the water and salt make a two-phase solution consisting of a solid (crystalline) salt phase sedimented in the aqueous solution with salt concentration of 0.357. Finally, after all water evaporates, only salt remains, which, together with dry protein, constitutes a droplet residue of mass

$$m_* = m_{\mathrm{s}} + m_{\mathrm{p}} = (f_{\mathrm{s}} + f_{\mathrm{p}})m_0 . \tag{3.7}$$

3.1 Density of the evaporating droplet

As the respiratory droplet looses water by evaporation, its density increases. This affects the motion, as seen from eqs. (2.6) in which the density ρ appears in the denominator of both equations. We therefore proceed to determine the density of the droplet as a function of time. The initial radius of the droplet R_0 and, thus, its initial volume $V_0 = 4\pi R_0^3/3$, are assumed to be known. If the rate of evaporation is specified by (3.5), the volume of the droplet at an arbitrary instant of evaporation is

$$V(t) = \frac{4\pi}{3}\,R^3(t), \quad R(t) = R_0\left(1 - \frac{t}{\tau}\right)^{1/2}, \quad \tau = \frac{4\pi R_0^2}{s} . \tag{3.8}$$

The density expression will be first derived for the stage of the evaporation process during which the concentration of dissolved salt in water is below the saturation value of 0.357. At an arbitrary instant during this stage of evaporation, the mass of the droplet is

$$m = m_{\mathrm{sol}}^{\mathrm{aq}} + m_{\mathrm{p}} = m_{\mathrm{sol}}^{\mathrm{aq}} + f_{\mathrm{p}} m_0 , \quad m_{\mathrm{sol}}^{\mathrm{aq}} = m_{\mathrm{w}} + m_{\mathrm{s}} = m_{\mathrm{w}} + f_{\mathrm{s}} m_0 . \tag{3.9}$$

Furthermore, the volume of the droplet is taken to be the sum of the volumes of the protein and the aqueous salt solution, i.e.,

$$V = V_{\mathrm{sol}}^{\mathrm{aq}} + V_{\mathrm{p}} = V_{\mathrm{sol}}^{\mathrm{aq}} + \frac{m_{\mathrm{p}}}{\rho_{\mathrm{p}}}, \quad \rho_{\mathrm{p}} = 1,350\,\mathrm{kg/m^3} . \tag{3.10}$$

The mass density of the dry protein is $\rho_{\mathrm{p}} = 1,350\,\mathrm{kg/m^3}$, as frequently adopted in the literature (e.g., Fisher et al., 2004), and is considered to be constant. Thus, from (3.10),

$$V_{\mathrm{sol}}^{\mathrm{aq}} = V - \frac{f_{\mathrm{p}}}{\rho_{\mathrm{p}}}\,m_0 . \tag{3.11}$$

The initial mass of the droplet m_0 is still unknown, because we assumed that only the initial droplet's volume V_0 is given (as, for example, obtained by the measurement of the initial droplet's radius), although one may reasonably expect that m_0 is nearly equal to $\rho_{\rm w}V_0$, because of the small initial weight percents of salt and protein. By introducing the mass density of the aqueous salt solution ($\rho^{\rm aq}_{\rm sol}$), we can write

$$m^{\rm aq}_{\rm sol} = \rho^{\rm aq}_{\rm sol} V^{\rm aq}_{\rm sol}\,, \tag{3.12}$$

and the substitution of (3.6) and (3.11) into (3.12) gives the quadratic equation for $m^{\rm aq}_{\rm sol}$,

$$(m^{\rm aq}_{\rm sol})^2 - b\, m^{\rm aq}_{\rm sol} - c = 0 \quad \Rightarrow \quad m^{\rm aq}_{\rm sol} = \frac{1}{2}\left(b + \sqrt{b^2+4c}\right), \tag{3.13}$$

where

$$b = \rho_{\rm w}\left(V - f_{\rm p}\,\frac{\rho_0}{\rho_{\rm p}}\,V_0\right), \quad c = \kappa f_{\rm s}\rho_0 V_0\left(V - f_{\rm p}\,\frac{\rho_0}{\rho_{\rm p}}\,V_0\right). \tag{3.14}$$

To determine the initial density ρ_0, we apply (3.13) to the initial instant when $(m^{\rm aq}_{\rm sol})^0 = m_0 - m_{\rm p} = (1-f_{\rm p})m_0 = (1-f_{\rm p})\rho_0 V_0$. Upon solving for ρ_0, it follows that

$$\rho_0 = \frac{(1-f_{\rm p})\rho_{\rm w} + \kappa f_{\rm s}}{(1-f_{\rm p})^2 + f_{\rm p}(1-f_{\rm p})\rho_{\rm w}/\rho_{\rm p} + \kappa f_{\rm s} f_{\rm p}/\rho_{\rm p}}\,. \tag{3.15}$$

By substituting $f_{\rm s} = f_{\rm p} = 0.01$, $\rho_{\rm w} = 997\,{\rm kg/m^3}$, $\rho_{\rm p} = 1,350\,{\rm kg/m^3}$, and $\kappa = 775\,{\rm kg/m^3}$, the initial density of the droplet is found to be $\rho_0 = 1,007.2\,{\rm kg/m^3}$. The corresponding initial mass of the droplet is then $m_0 = \rho_0 V_0$. It is noted that the initial 98 wt% of water content is equivalent to an initial 99 vol% of water, which is obtained by multiplying 98 with $\rho_0/\rho_{\rm w} = 1007.2/997 = 1.01$. Consequently, the initial 2 wt% of salt and protein together is equivalent to only 1 vol% of their initial volume content.

Expressions (3.13) and (3.14) specify the mass $m^{\rm aq}_{\rm sol} = m^{\rm aq}_{\rm sol}(V_0, V)$ in terms of the known V_0 and V, and all the other known parameters that appear in these expressions. The density of the aqueous salt solution follows from (3.6) and is

$$\rho^{\rm aq}_{\rm sol} = \rho_{\rm w} + \kappa\, f_{\rm s}\frac{\rho_0 V_0}{m^{\rm aq}_{\rm sol}}\,, \tag{3.16}$$

where $m^{\rm aq}_{\rm sol}$ is given by (3.13) and (3.14). In particular, it follows that $(\rho^{\rm aq}_{\rm sol})^0 = 1,004.6\,{\rm kg/m^3}$.

Finally, the total mass of the droplet is obtained by substituting (3.13) into (3.9). This gives

$$m = m^{\rm aq}_{\rm sol} + m_{\rm p} = m^{\rm aq}_{\rm sol} + f_{\rm p}\rho_0 V_0\,, \tag{3.17}$$

with the corresponding density

$$\rho = \frac{m}{V} = \frac{m^{\rm aq}_{\rm sol}}{V} + f_{\rm p}\rho_0\,\frac{V_0}{V}\,, \tag{3.18}$$

where, again, $m^{\rm aq}_{\rm sol}$ is as specified in (3.13) and (3.14).

The saturation point of the aqueous salt solution is reached when $m^{\rm aq}_{\rm sol}$ decreases to the value $\hat{m}^{\rm aq}_{\rm sol}$, such that

$$\frac{m_{\rm s}}{\hat{m}^{\rm aq}_{\rm sol}} = 0.357 \quad \Rightarrow \quad \hat{m}^{\rm aq}_{\rm sol} = \frac{m_{\rm s}}{0.357} = \frac{f_{\rm s}m_0}{0.357} = 0.028 m_0\,. \tag{3.19}$$

The corresponding density of the saturated aqueous solution is, from (3.6),

$$\hat{\rho}^{\rm aq}_{\rm sol} = \rho_{\rm w} + \kappa\,\frac{m_{\rm s}}{\hat{m}^{\rm aq}_{\rm sol}} = \rho_{\rm w} + 0.357\kappa = 1,273.7\,{\rm kg/m^3}\,, \tag{3.20}$$

while its volume is

$$\hat{V}^{\rm aq}_{\rm sol} = \frac{\hat{m}^{\rm aq}_{\rm sol}}{\hat{\rho}^{\rm aq}_{\rm sol}} = 0.0222 V_0\,. \tag{3.21}$$

The mass, volume, and density of the entire droplet at this instant are

$$\begin{aligned}\hat{m} &= \hat{m}_{\rm sol}^{\rm aq} + m_{\rm p} = \frac{f_{\rm s} m_0}{0.357} + f_{\rm p} m_0 = 0.038 m_0\,,\\ \hat{V} &= \hat{V}_{\rm sol}^{\rm aq} + V_{\rm p} = \hat{V}_{\rm sol}^{\rm aq} + \frac{f_{\rm p}\rho_0 V_0}{\rho_{\rm p}} = 0.03 V_0\,,\\ \hat{\rho} &= \frac{\hat{m}}{\hat{V}} = 1.2795\rho_0 = 1,288.7\,{\rm kg/m^3}\,.\end{aligned} \tag{3.22}$$

The corresponding radius of the droplet and its bounding surface are

$$\hat{R} = \left(\frac{3\hat{V}}{4\pi}\right)^{1/3} = 0.31 R_0\,, \quad \hat{S} = 4\pi\hat{R}^2 = 0.096 S_0\,. \tag{3.23}$$

Consequently, from (3.5), the time at the instant of saturation is

$$\hat{t} = \frac{S_0 - \hat{S}}{s} = \frac{0.904 S_0}{s} = 0.904\tau\,, \quad \tau = S_0/s\,. \tag{3.24}$$

The parameter s depends on the relative humidity as defined in (3.4).

3.2 Density expressions after saturation of aqueous salt solution

As the water continues to evaporate beyond the saturation time $\hat{t}$ given by (3.22), a portion of the total salt amount $m_{\rm s}$ (denoted by $m_{\rm s}''$) precipitates, and the remaining portion of salt $m_{\rm s}' = 0.357 m_{\rm sol}^{\rm sat}$ is dissolved in the saturated aqueous solution, so that $m_{\rm s} = m_{\rm s}' + m_{\rm s}''$. The total mass of the droplet at this stage of evaporation is, thus,

$$m = m_{\rm sol}^{\rm sat} + m_{\rm s}'' + m_{\rm p} = m_{\rm sol}^{\rm sat} + (m_{\rm s} - m_{\rm s}') + m_{\rm p} = 0.643 m_{\rm sol}^{\rm sat} + m_{\rm s} + m_{\rm p}\,. \tag{3.25}$$

Furthermore, the volume of the droplet is

$$V = V_{\rm sol}^{\rm sat} + V_{\rm s}'' + V_{\rm p} = \frac{m_{\rm sol}^{\rm sat}}{\hat{\rho}_{\rm sol}^{\rm aq}} + \frac{m_{\rm s}''}{\rho_{\rm s}} + \frac{m_{\rm p}}{\rho_{\rm p}} = \frac{m_{\rm sol}^{\rm sat}}{\hat{\rho}_{\rm sol}^{\rm aq}} + \frac{m_{\rm s} - 0.357 m_{\rm sol}^{\rm sat}}{\rho_{\rm s}} + \frac{m_{\rm p}}{\rho_{\rm p}}\,, \tag{3.26}$$

where $\hat{\rho}_{\rm sol}^{\rm aq} = 1,273.7\,{\rm kg/m^3}$, as determined in (3.20), and $\rho_{\rm s} = 2,160\,{\rm kg/m^3}$ is the density of solid (crystalline) NaCl. Equation (3.26) can be solved for $m_{\rm sol}^{\rm sat}$ to obtain

$$m_{\rm sol}^{\rm sat} = \hat{\rho}_{\rm sol}^{\rm aq}\,\frac{V - m_{\rm s}/\rho_{\rm s} - m_{\rm p}/\rho_{\rm p}}{1 - 0.357\,\hat{\rho}_{\rm sol}^{\rm aq}/\rho_{\rm s}}, \tag{3.27}$$

where $m_{\rm s} = f_{\rm s} m_0$, $m_{\rm p} = f_{\rm p} m_0$, $m_0 = \rho_0 V_0$, and V is still given by (3.8). With the numerical values substituted, (3.27) becomes

$$m_{\rm sol}^{\rm sat} = \alpha_1 V - \beta_1 V_0\,, \quad \alpha_1 = 1,613\,{\rm kg/m^3}\,, \quad \beta_1 = 19.559\,{\rm kg/m^3}\,. \tag{3.28}$$

By substituting (3.27) into (3.25), we obtain

$$m = \alpha V + \beta V_0\,, \tag{3.29}$$

where

$$\alpha = \frac{0.643\hat{\rho}_{\rm sol}^{\rm aq}}{1 - 0.357\,\hat{\rho}_{\rm sol}^{\rm aq}/\rho_{\rm s}}, \quad \beta = \rho_0\left(f_{\rm s} + f_{\rm p} - 0.643\,\hat{\rho}_{\rm sol}^{\rm aq}\,\frac{f_{\rm s}/\rho_{\rm s} + f_{\rm p}/\rho_{\rm p}}{1 - 0.357\,\hat{\rho}_{\rm sol}^{\rm aq}/\rho_{\rm s}}\right). \tag{3.30}$$

The numerical values for α and β are $\alpha = 1,030\,{\rm kg/m^3}$ and $\beta = 7.657\,{\rm kg/m^3}$. Finally, the density of the droplet during this stage of its evaporation is, from (3.29),

$$\rho = \frac{m}{V} = \alpha + \beta \frac{V_0}{V} \,. \tag{3.31}$$

3.3 Size of the droplet's residue

If all water evaporates and only salt and dry protein remain in their original amount, the mass of the droplet's residue is $m_* = m_\mathrm{s} + m_\mathrm{p}$, as given in (3.7). (Proteins in aqueous solutions bind some of the water molecules very firmly, but in our model we consider that all the droplet's water can eventually evaporate during the droplet's motion in the air.) According to (3.29), m_* must be equal to $\alpha V_* + \beta V_0$, where V_* is the volume of the droplet's residue, i.e.,

$$\alpha V_* + \beta V_0 = (f_\mathrm{s} + f_\mathrm{p})\rho_0 V_0 \,. \tag{3.32}$$

Thus,

$$V_* = \frac{1}{\alpha}\,[(f_\mathrm{s} + f_\mathrm{p})\rho_0 - \beta]V_0 = 0.0121 V_0 \,. \tag{3.33}$$

The average density of the droplet's residue is

$$\rho_* = \frac{m_*}{V_*} = \frac{(f_\mathrm{s} + f_\mathrm{p})\rho_0 \alpha}{(f_\mathrm{s} + f_\mathrm{p})\rho_0 - \beta} = 1.6496\rho_0 = 1,661.5\,\mathrm{kg/m^3} \,, \tag{3.34}$$

while the corresponding radius and surface area are

$$R_* = \left(\frac{2V_*}{4\pi}\right)^{1/3} = \sqrt[3]{0.0121}\, R_0 = 0.23 R_0 \,, \quad S_* = 4\pi R_*^2 = 0.6625 S_0 \,. \tag{3.35}$$

The time at the instant when the droplet reaches its residue (nucleus) size is

$$t_* = \frac{S_0 - S_*}{s} = 0.3375\tau \,, \quad \tau = S_0/s \,. \tag{3.36}$$

We note that the residue's density can also be derived directly from the additive mass and volume expressions

$$\begin{aligned} m_* &= \rho_* V_* = m_\mathrm{s} + m_\mathrm{p} = (f_\mathrm{s} + f_\mathrm{p}) m_0 \,, \\ V_* &= V_\mathrm{s} + V_\mathrm{p} = \frac{m_\mathrm{s}}{\rho_\mathrm{s}} + \frac{m_\mathrm{p}}{\rho_\mathrm{p}} = \left(\frac{f_\mathrm{s}}{\rho_\mathrm{s}} + \frac{f_\mathrm{p}}{\rho_\mathrm{p}}\right)\rho_0 V_0, \end{aligned} \tag{3.37}$$

from which it follows that the density of the residue particle is

$$\rho_* = \frac{m_*}{V_*} = \frac{m_\mathrm{s} + m_\mathrm{p}}{m_\mathrm{s}/\rho_\mathrm{s} + m_\mathrm{p}/\rho_\mathrm{p}} = \frac{f_\mathrm{s} + f_\mathrm{p}}{f_\mathrm{s}/\rho_\mathrm{s} + f_\mathrm{p}/\rho_\mathrm{p}} \,. \tag{3.38}$$

4 Numerical results

Figure 2 shows the variations of the radius, surface, mass, and density of an evaporating droplet of initial radius $R_0 = 25\,\mu$m under four indicated values of relative humidity. The initial mass of the droplet is $m_0 = 6.592 \times 10^{-11}$ kg and its average density is $\rho_0 = 1,007.2\,\mathrm{kg/m^3}$. The initial mass of the aqueous salt solution of the droplet is $(m_\mathrm{sol}^\mathrm{aq})^0 = 6.526 \times 10^{-11}$ kg and its density $(\rho_\mathrm{sol}^\mathrm{aq})^0 = 1,004.6\,\mathrm{kg/m^3}$. When the aqueous salt solution becomes saturated, its mass, volume, and density are $\hat{m}_\mathrm{sol}^\mathrm{aq} = 1.8465 \times 10^{-12}$ kg, $\hat{V}_\mathrm{sol}^\mathrm{aq} = 1.458 \times 10^{-15}\,\mathrm{m^3}$, and $\hat{\rho}_\mathrm{sol}^\mathrm{aq} = 1,266.5\,\mathrm{kg/m^3}$, respectively. The corresponding radius, mass, volume, and density of the entire droplet at that instant are $\hat{R} = 0.31 R_0 = 7.745\,\mu$m, $\hat{m} = 0.038 m_0 = 2.506 \times 10^{-12}$ kg, $\hat{V} = 0.03 V_0 = 1.946 \times 10^{-15}\,\mathrm{m^3}$, and $\hat{\rho} = 1.278\rho_0 = 1,287.5\,\mathrm{kg/m^3}$. At the instant when all the water evaporates and the droplet reduces to its residue size, its radius is $R_* = 0.23 R_0 = 5.743\,\mu$m. The corresponding mass, volume, and density are $m_* = 0.02 m_0 = 1.318 \times 10^{-12}$ kg, $V_* = 0.0121 V_0 = 7.935 \times 10^{-16}\,\mathrm{m^3}$, and $\rho_* = 1.6496\rho_0 = 1,661.5\,\mathrm{kg/m^3}$.

The times for the aqueous salt solution to reach its saturation state and for the droplet to reach its residue state depend on the relative humidity. For relative humidities of 0%, 25%, 50%, 75%, these times are $\hat{t}$ =2.18, 2.91, 4.37, 8.74 seconds and t_* =2.29, 3.05, 4.58, 9.16 seconds, respectively. These values are for $R_0 = 25\,\mu$m; the results for other values of the initial radius follow similarly. The times $\hat{t}$ and t_* increase with the increase of the initial radius. For example, for a droplet of initial radius $R_0 = 50\,\mu$m, the times are $\hat{t}$ =8.74, 11.65, 17.48, 34.96 seconds and t_* =9.16, 12.21, 18.31, 36.62 seconds, respectively. Depending on the height from which the droplet is emitted, these times may be much longer than the times it takes a droplet to reach the ground. This is discussed below.

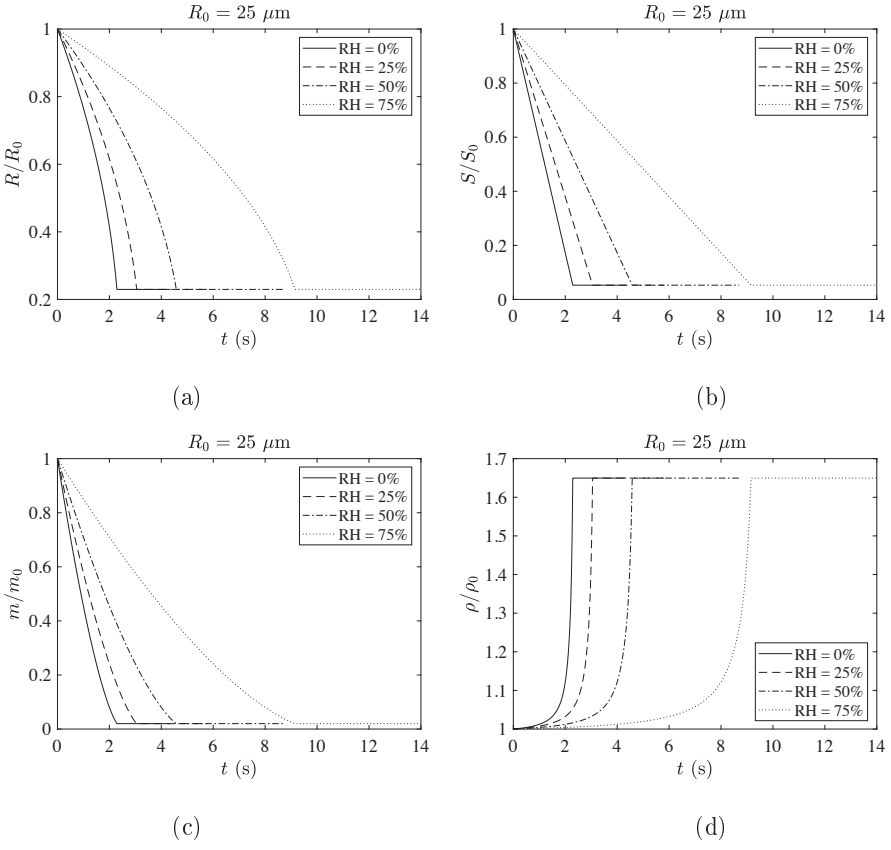

Figure 2: The variation of the (a) radius, (b) surface, (c) mass, and (d) density of an evaporating droplet with initial radius $R_0 = 25\mu$m under four different relative humidities.

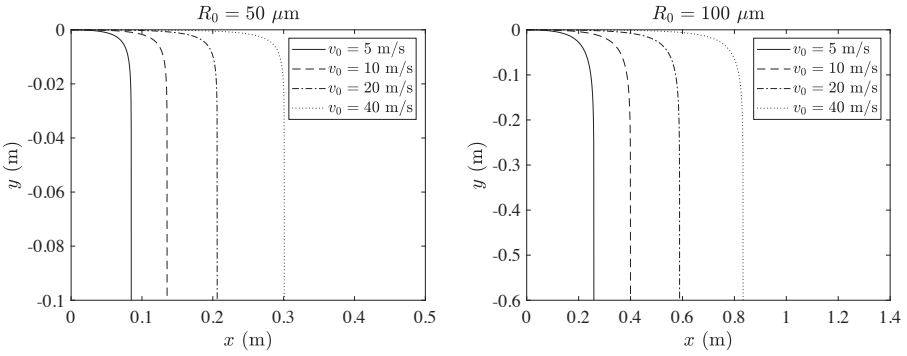

(a) (b)

Figure 3: The trajectories of droplets of initial radii $R_0 = 50$ and 100 μm, ejected horizontally with the velocities $v_0 = 5$, 10, 20 and 40 m/s, under the relative humidity RH = 25%. Upon reaching its maximum horizontal distance, the droplet falls vertically downwards.

Figure 3 shows the trajectories of the droplets of initial radii $R_0 = 50$ and 100 μm, emitted horizontally from the mouth with initial velocities $v_0 = 5$, 10, 20, and 40 m/s, in stagnant air under a relative humidity of 25%. Figure 4 shows the plots $x = x(t)$ and $y = y(t)$ for droplets with initial radii $R_0 = 50$ and 100 μm under the same relative humidity of 25%. The vicinity of the maximum horizontal distance is rapidly reached, which is followed by an essentially vertical descent of the droplet. The maximum horizontal distance is strongly dependent on the magnitude of the initial horizontal velocity v_0, while the time variation $y = y(t)$ is only mildly affected by v_0.

For the 50 μm initial radius, the droplet evaporates to its 11.5 μm radius residue in about 12.2 seconds. This is followed by an essentially vertical fall of the non-evaporating residue toward the ground (Fig. 4a), with its velocity approaching the terminal velocity $(2/9)R_*^2\rho g/\eta_{\rm air} = 2.62$ cm/s. If the ground is 2 m below the point of exhalation, then the droplet reaches the ground in about 21 seconds, i.e., about 9.5 seconds after it reaches its residue (nucleus) size. On the other hand, the 100 μm initial radius droplet is sufficiently large to reach the ground, 2 m below the point of exhalation, in just 3 seconds, which is far shorter than 49 seconds that would be needed to evaporate to its residue size of about 23 μm radius (Fig. 4d).

Figures 3 and 4 also quantify how much further the droplet moves horizontally upon coughing ($v_0 = 40$ m/s) comparing to soft talking ($v_0 = 5$ m/s). For example, the maximum horizontal reach of the droplet with initial radius 100 μm is about 83 cm in the case $v_0 = 40$ m/s, while it is just about 26 cm in the case $v_0 = 5$ m/s (both at a relative humidity of 25%). For the initial droplet's radius of 50 μm, the maximum horizontal reach is about 30 cm in the case $v_0 = 40$ m/s, while it is less than 1/3 of that (8.5 cm) in the case $v_0 = 5$ m/s.

Figure 5 shows the effect of the rate of evaporation s_0 on the time-variation of the droplet's position. Three values of s_0 are used in the plots, $s_0 = s_\bullet = 3.25 \times 10^{-9}$ m^2/s, $s_0 = (2/3)s_\bullet$, and $s_0 = (4/3)s_\bullet$. The horizontal position (x coordinate) is very little affected by s_0, as the droplet rapidly looses (within less than 0.2 seconds) its horizontal momentum due to aerodynamic drag,

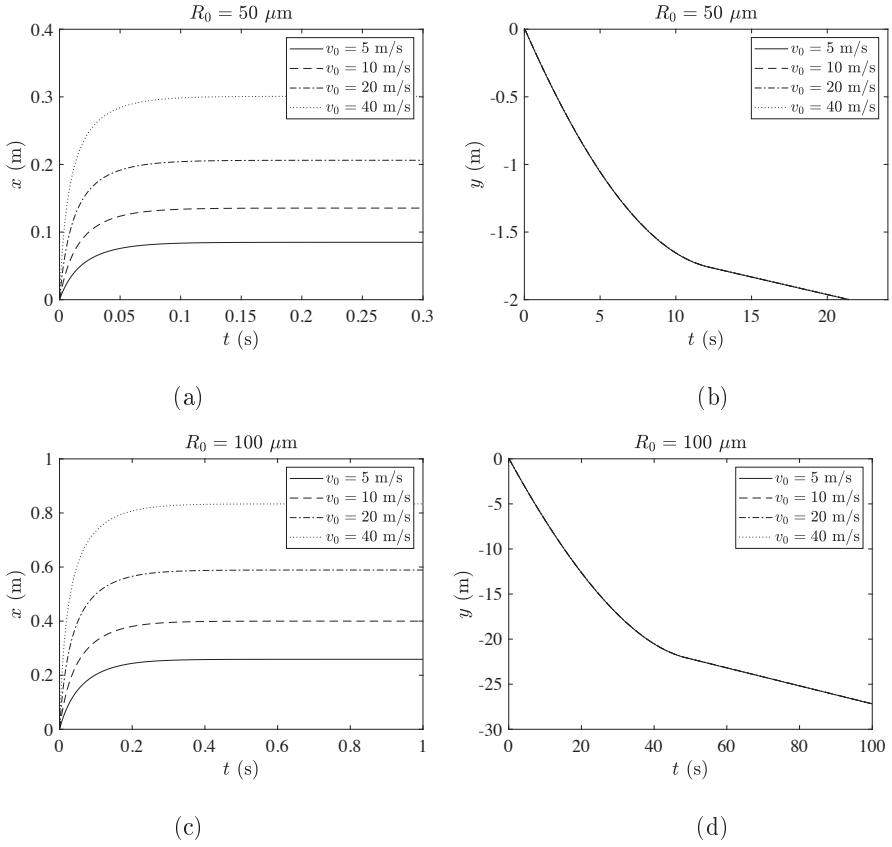

Figure 4: The variation of the x and y coordinates of the droplet's trajectory with time t for droplets of initial radii $R_0 = 50$ (parts a and b), and 100 μm (parts c and d), ejected horizontally with the velocities $v_0 = 5$, 10, 20 and 40 m/s, under the relative humidity RH = 25%.

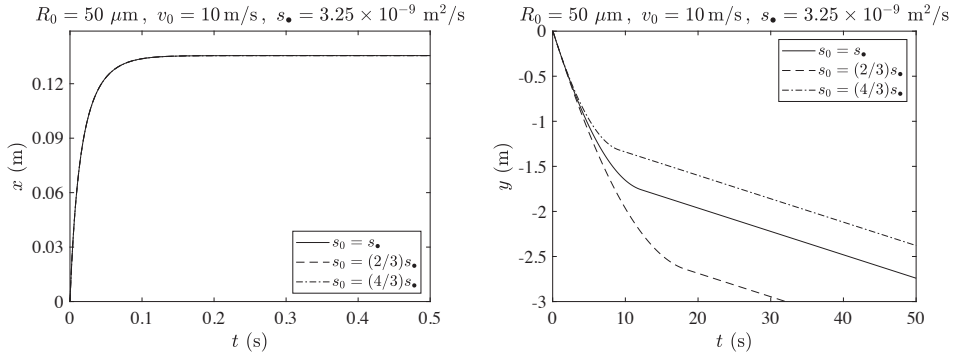

(a) (b)

Figure 5: The effect of the rate of evaporation s_0 on the time variation of the droplet's (x, y) coordinates. (a) The x coordinate is affected very little by the change of s_0. (b) The y coordinate is affected substantially as the droplet descends vertically and reaches its nucleus size much sooner for higher values of s_0. The relative humidity is RH = 25%.

before any substantial evaporation takes place. The vertical position (y coordinate) is, however, affected substantially by the change of s_0, as the droplet descends vertically by the action of gravity, while its size and weight substantially decrease due to evaporation. The droplet reaches its nucleus size (the kink in the curves shown in Fig. 5) much sooner for higher values of s_0. The time it takes for the droplet of initial radius 50 μm, ejected at the speed of 10 m/s, to descend by 2 m is about 10 seconds in the case $s_0 = (2/3)s_\bullet$, 21 seconds in the case $s_0 = s_\bullet$, and 35 seconds in the case $s_0 = (4/3)s_\bullet$. The relative humidity in all three cases is assumed to be the same (RH=25%). Thus, at higher ambient temperature (higher value of s_0), the droplet remains in the air at a higher height longer, which increases the risk of infection (more rapidly evaporating droplets are lighter and fall to the ground slower).

Finally, Fig. 6 shows the trajectories of a droplet of initial radius 100 μm, ejected with initial velocities $v_0 = 5$, 10, 20 and 40 m/s under a relative humidity of 25% at the angles $\varphi_0 = \pm 30^\circ$ and $\pm 45^\circ$. The results illustrate the effect of the initial angle on the horizontal reach of the droplet. This is of importance because a person can, for example, speak while sitting in the chair next to the person standing by the chair, or vice versa. Clearly, the maximum reach increases with the decrease of the magnitude of the angle φ_0, being the greatest for $\varphi_0 = 0^\circ$. These numerical results are of importance for the evaluation of the risks of infection by transmitted pathogenic droplets and the estimates of safe distancing while communicating during standing and/or sitting, or from different elevations and heights. For example, the maximum vertical reach of a 100 μm-radius droplet ejected by soft talking with $v_0 = 5$ m/s at $\varphi_0 = 45^\circ$ is $y_{\max} = 11.6$ cm, while its maximum horizontal reach is $x_{\max} = 19.3$ cm. On the other hand, the maximum vertical reach of the same droplet ejected by coughing with $v_0 = 40$ m/s is $y_{\max} = 51.2$ m, while its maximum horizontal reach is $x_{\max} = 60.3$ cm. If the droplet was ejected horizontally ($\varphi_0 = 0^\circ$), the maximum horizontal reach would have been 25.9 cm in soft talking and 83.4 cm in coughing (Fig. 3d).

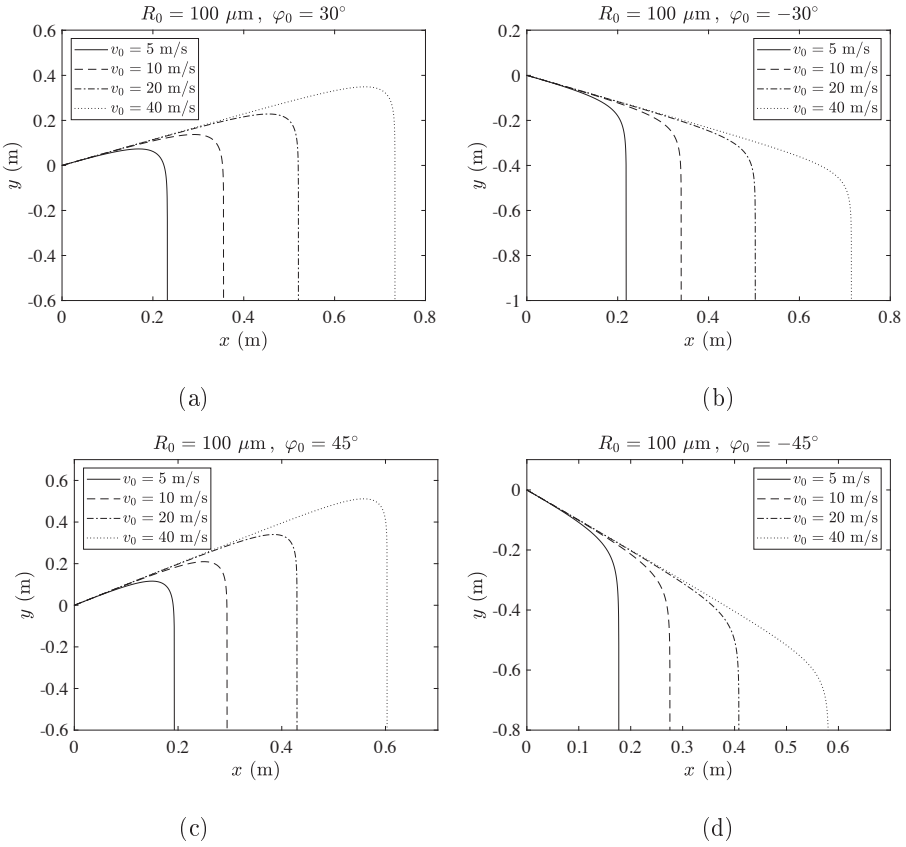

Figure 6: The trajectories of the droplet of initial radius 100 μm, ejected from mouth with the velocities $v_0 = 5$, 10, 20 and 40 m/s at the angles $\varphi_0 = \pm 30^\circ$ and $\pm 45^\circ$. The relative humidity is RH = 25%.

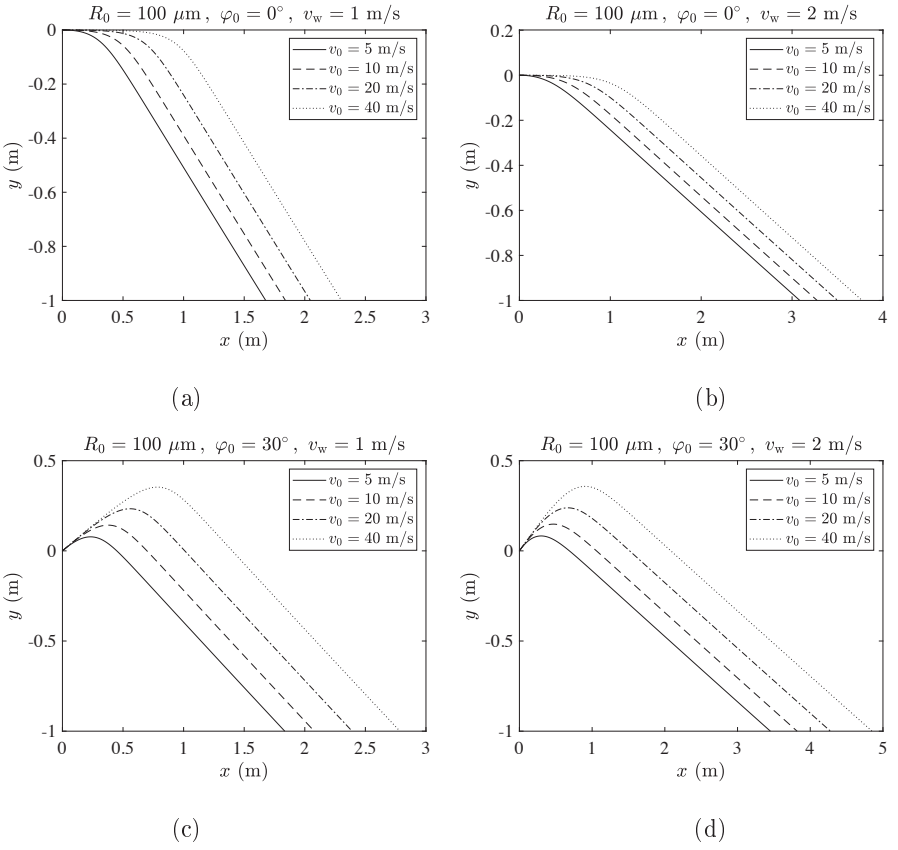

Figure 7: The trajectories of a droplet of initial radius 100 μm, ejected with the velocities $v_0 = 5$, 10, 20 and 40 m/s at the angle $\varphi_0 = 0$ in parts (a) and (b), and $\varphi_0 = 30^\circ$ in parts (c) and (d). The wind velocity in parts (a) and (c) is 1 m/s, and 2 m/s in parts (b) and (d). The relative humidity is RH = 25%.

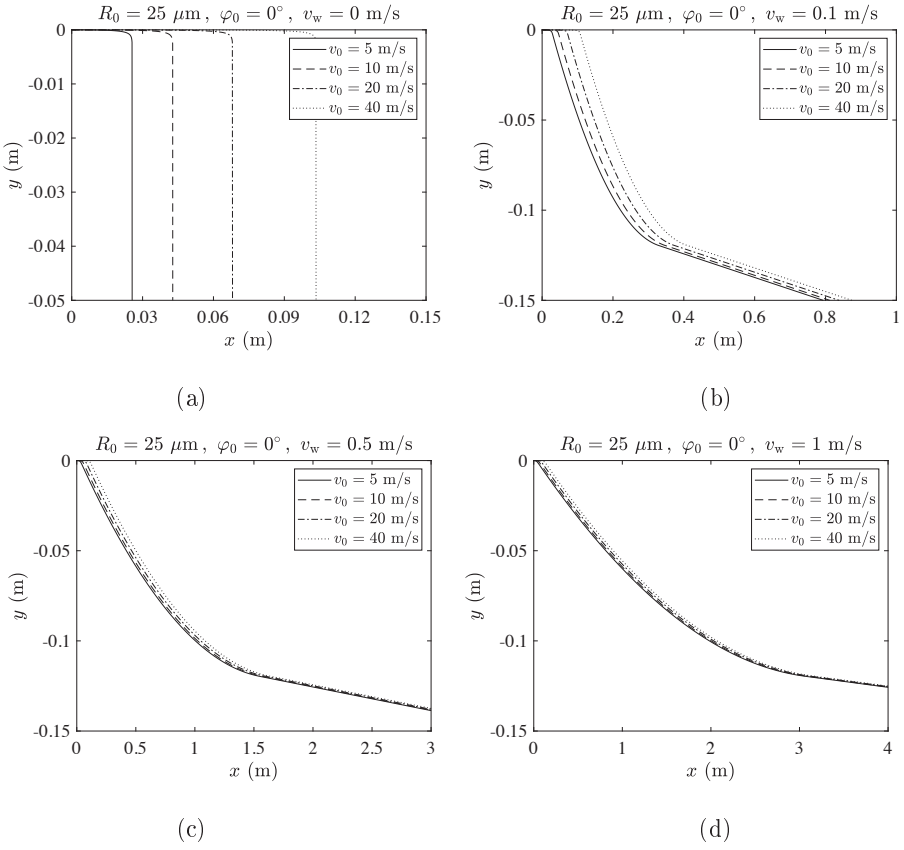

Figure 8: The trajectories of a droplet of initial radius 25 μm, ejected horizontally with the velocities $v_0 = 5$, 10, 20 and 40 m/s. The wind is absent in part (a), while the wind velocity in parts (b), (c), and (d) is 0.1, 0.5, and 1 m/s, respectively. The relative humidity is RH = 25%.

5 Wind effects

The projectile motion considered in previous sections was assumed to take place under quiescent ambient conditions without any external air flow. The effect of external air flow (wind or ventilation) can be readily included in the analysis. For example, if the wind is horizontal, with a constant speed $v_{\rm w}$, the equations of motion are given by (2.6), with v_x replaced by $v_x - v_{\rm w}$, and v by $[(v_x - v_{\rm w})^2 + v_y^2]^{1/2}$, while the Reynolds number in (2.3) becomes ${\rm Re} = 2R[(v_x - v_{\rm w})^2 + v_y^2]^{1/2}/\nu_{\rm air}$. Figure 7 shows the the trajectories of a droplet of initial radius $R_0 = 100\,\mu$m, ejected with four indicated initial velocities in the case of forward wind with speed 1 m/s and 2 m/s. The relative humidity in all cases is assumed to be the same and equal to RH=25%. In Fig. 7a and 7b, the droplet is ejected horizontally, and in Fig. 7c and 7d the ejection angle is $\varphi_0 = 30^\circ$. If these trajectories are compared with the trajectories shown in Fig. 3b and Fig. 6a without wind, we can see that the presence of wind greatly affects the shape of the trajectory and the maximum horizontal reach of the droplet. Similarly, Fig. 8 shows the comparison of the trajectories of a droplet with an initial radius of only 25 μm, ejected horizontally in the absence of wind and in the direction of wind whose velocity is 0.1, 0.5, and 1 m/s. While the maximum horizontal distance in the absence of wind is only about 2.5 to 10.4 cm (depending on the ejection velocity v_0), in the presence of even a mild wind the horizontal reach of the droplet may extend to several meters, while the vertical descent is only about 15 cm. This naturally contributes to the increase of the infection spreading risk, if the droplets carry viruses or other pathogens. A recent numerical study of the influence of wind on the COVID-19 airborne transmission has been presented by Feng et al. (2020).

5.1 Droplet's motion against the wind

Figure 9 shows the trajectories of the droplet of initial radius 100 μm, considered in Fig. 7, but now in the case of reversed wind direction. Upon its initial forward motion, the droplet reverses the direction of its motion and moves backward. Note that, in the case of $\varphi_0 = 45^\circ$, the reversal of the direction of motion takes place below the line along the direction of the initial droplet velocity $\rm v_0$ for the wind speed $v_{\rm w} = -0.5$ m/s, and above that line for the wind speed $v_{\rm w} = -1$ m/s. From all four plots in Fig. 9 it follows that a droplet emitted by a taller person against the wind can easily reach a person standing behind even at distances beyond one or two meters, particularly at stronger winds.

Figure 10a shows the trajectory of the droplet of initial radius 100 μm, ejected at $\varphi_0 = 45^\circ$ with the initial velocity $v_0 = 10$ m/s against the wind with velocity $v_{\rm w} = -1$ m/s. Upon quick reversal of its direction of motion, the droplet falls to the ground, 2 meters below the point of ejection, in just 3.2 seconds, far before the droplet would reach its nucleus size of $23\,\mu$m (in 49 seconds). Figure 10b shows the time variations $x = x(t)$ and $y = y(t)$ during the first 3.5 seconds. The corresponding variations of the velocity components $v_x = v_x(t)$ and $v_y = v_y(t)$ are shown in Fig. 10c. The horizontal component of the droplet's velocity quickly approaches the value of the wind velocity (-0.1 m/s), while the vertical component asymptotically approaches the value of the terminal velocity $v_{\rm t} = 0.01$ m/s, albeit in a much longer time (not shown in Fig. 10c). The slope of the trajectory at such large times would be given by the ratio $-v_{\rm t}/v_{\rm w}$. The variations of the Reynolds number Re and the drag coefficient $c_{\rm d}$ with time (on the logarithmic scale, and extended to more than 1,000 seconds) are shown in Fig. 10d. Only the early portion of Fig. 10d is relevant for the droplet's descent of the order of several or even several tens of meters, because the droplet would descend by 20 m in less than 40 seconds, if not interrupted by the ground or another barrier.

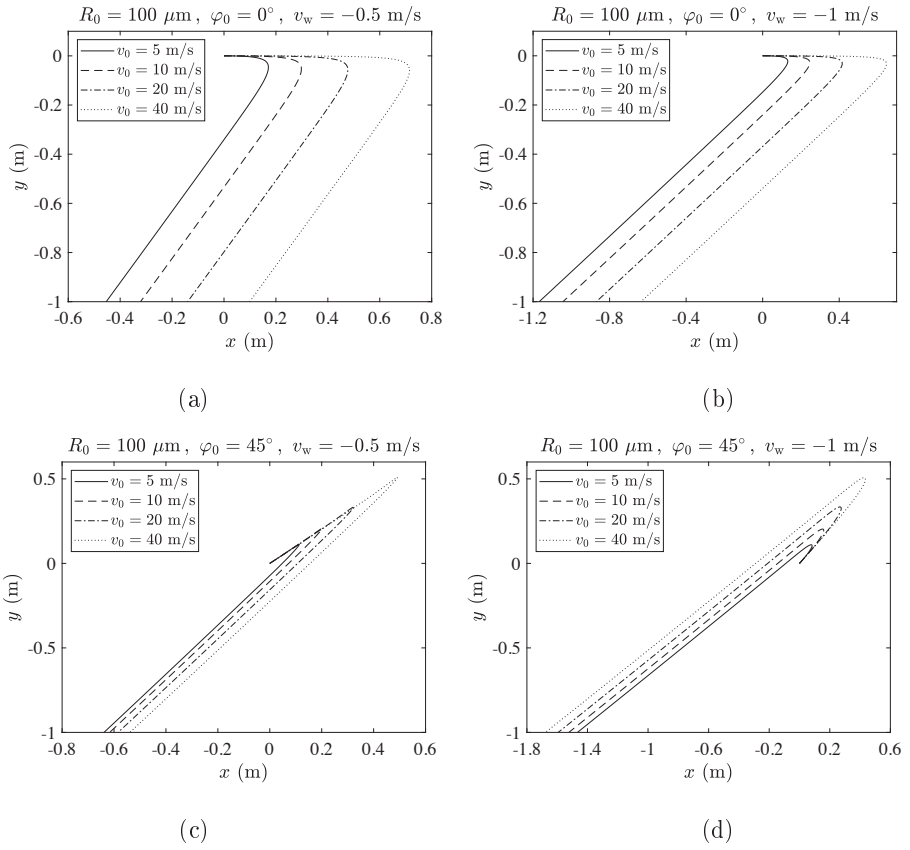

Figure 9: The trajectories of a droplet of initial radius 100 μm, ejected with the velocities $v_0 = 5$, 10, 20 and 40 m/s against the horizontal wind. The direction of v_0 is at the angle $\varphi_0 = 0$ in parts (a) and (b), and $\varphi_0 = 45^\circ$ in parts (c) and (d). The wind velocity in parts (a) and (c) is -0.5 m/s, and -1 m/s in parts (b) and (d). The relative humidity is RH = 25%.

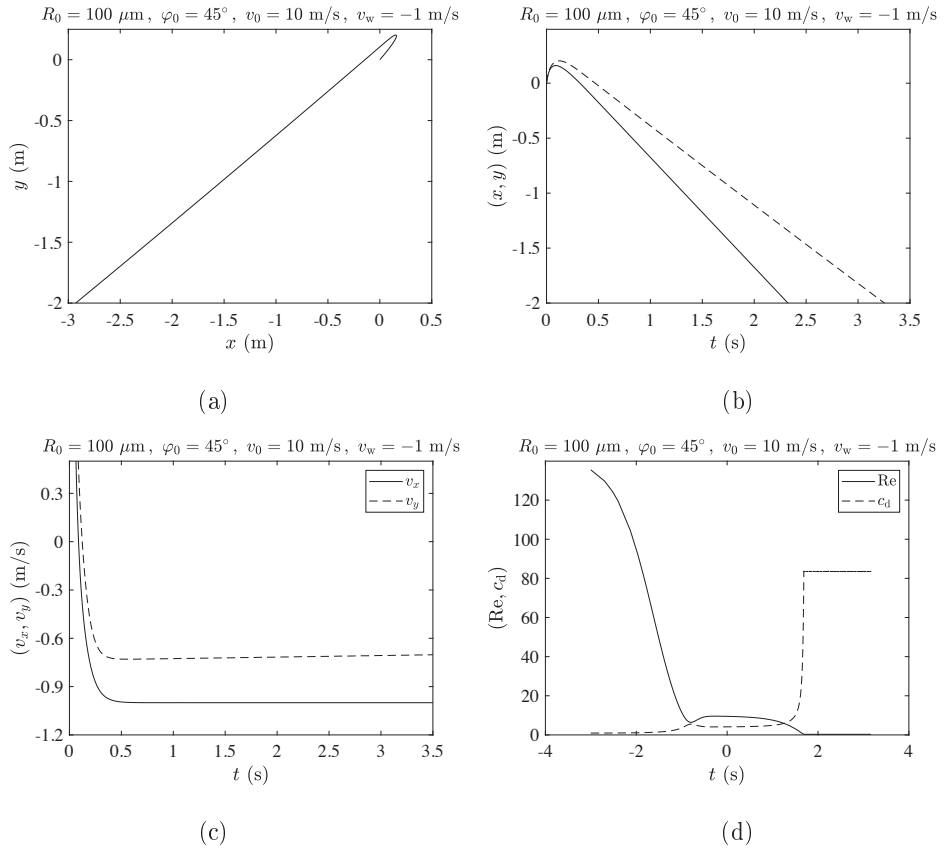

Figure 10: (a) The trajectory $y = y(x)$ of a droplet of initial radius 100 μm, ejected with the velocity $v_0 = 10$ m/s at the angle $\varphi_0 = 45^\circ$ against the horizontal wind $v_w = -1$ m/s, under the relative humidity RH = 25%. The corresponding time variations of (b) the coordinates $x = x(t)$ and $y = y(t)$, and (c) the velocity components $v_x = v_x(t)$ and $v_y = v_y(t)$. (d) The variations of the Reynolds number and the drag coefficient in the extended time range (on the logarithmic scale).

6 Conclusions

We have presented an analysis of the projectile motion of a micro-droplet ejected from the mouth at an arbitrary angle and initial velocity, corresponding to soft or loud speaking, coughing or sneezing. It is assumed that a droplet is ejected as an isolated droplet, outside of the puff of exhaled air. The air resistance is represented by a drag force which is a nonlinear function of the droplet's velocity. The evaporation of the droplet is described by an expression based on the assumption that the rate of decrease of the droplet's external surface area is dependent only on the relative humidity and the ambient temperature. The initial content of the respiratory droplet is taken to be 98 wt% water, 1 wt% salt (NaCl), and 1 wt% protein (mucus). The change of the average density of the droplet caused by evaporation of its water is determined throughout the concentration range, up to the instant when all the water evaporates and the droplet reduces to its nucleus, consisting of salt and dry protein only. The presented density analysis also specifies the change of the droplet's mass during evaporation, which enables the numerical solution of the governing differential equations of the droplet's motion after its emission from the mouth. The trajectories of different-sized droplets ejected at different velocities and under different relative humidities are determined and discussed. In each considered case the maximum horizontal distance traveled by a droplet is rapidly reached, which is followed by an essentially vertical descent of the droplet in a stagnant air. A droplet's maximum horizontal reach is compared in the case of speaking vs. coughing or sneezing. The time needed for a droplet to evaporate down to its nucleus size is compared with the time for the droplet to reach the ground, after being ejected from a given height. The effect of the droplet's evaporation rate on its size and motion is quantified. More rapidly evaporating droplets are lighter and fall to the ground slower, which increases the risk of infection. The effects of the ejection angle of a droplet on its maximum horizontal and vertical reach and the entire trajectory are also evaluated and discussed, which is of importance for the analysis of transmission of infection in the cases when a person speaks while sitting near a standing person, or vice versa. The negative ejection angles are also of interest in studying the projectile motion of the droplets that have escaped from a moving puff. The wind effect on the droplet's trajectory and its maximum horizontal reach is also studied. For example, while the maximum horizontal distance of the droplet with 25 μm initial radius in the absence of wind is only about 3 to 10 cm, depending on the ejection velocity, in the presence of even a very mild wind the horizontal reach of the droplet extends to several meters. This naturally contributes to the increase of the risk of infection, if the droplets carry viruses or other pathogens. If an isolated droplet is ejected against the wind, subsequent to its initial forward motion, the droplet reverses the direction of its motion and moves backward. If a droplet is emitted by a taller person against the wind, it can easily reach a person standing behind even at distances beyond a meter, particularly at stronger winds. The analysis can be readily extended to include other in-plane wind directions. In the case of an out-of-plane wind (v_0 and v_w being non-coplanar), the projectile motion becomes three-dimensional, which will be discussed elsewhere. The motion of droplets that are trapped and carried by an exhaled air puff during its forward motion is more involved and not considered in this paper. The motion of small droplets relative to the puff is rather slow, and the model of linear drag may be adopted, but the main difficulty is the kinetic description of the moving and expanding puff which carries the small droplets, as discussed in a recent review by Balachandar et al. (2020) and the references cited therein.

References

Anchordoqui, L.A., Chudnovsky, E.M. (2020). A physicist view of COVID-19 airborne infection through convective airflow in indoor spaces. SciMedicine J., 2, 68–72. doi:10.28991/SciMedJ-2020-02-SI-5

Balachandar, S., Zaleski, S., Soldati, A., G. Ahmadi, G., Bourouiba, L. (2020). Host-to-host airborne transmission as a multiphase flow problem for science-based social distance guidelines. Int. J. Multiphase Flow, 132, Article 103439. doi:10.1016/j.ijmultiphaseflow.2020.103439

Bourouiba, L. (2020). Turbulent gas clouds and respiratory pathogen emissions: potential implications for reducing transmission of COVID-19. JAMA,323,1837–1838. doi:10.1001/jama.2020.4756

Chaudhuri, S., Basu, S., Kabi, P., Unni, V.R., Saha, A. (2020). Modeling the role of respiratory droplets in Covid-19 type pandemics. Phys. Fluids, 32, Article 063309. doi:10.1063/5.0015984

Chen, L.-D. (2020). Effects of ambient temperature and humidity on droplet lifetime - A perspective of exhalation sneeze droplets with COVID-19 virus transmission. Int. J. Hyg. Environ. Health, 229, Article 113568. doi:10.1016/j.ijheh.2020.113568

Cheng, C.H., Chow, C.L., Chow, W.K. (2020). Trajectories of large respiratory droplets in indoor environment: a simplified approach. Build. Environ., 183, Article 107196. doi:10.1016/j.buildenv.2020.107196

Das, S.K., Alam, J., Plumari, S., Greco, V. (2020). Transmission of airborne virus through sneezed and coughed droplets. Phys. Fluids, 32, Article 097102. doi:10.1063/5.0022859

Duguid, J.P. (1946). The size and the duration of air-carriage of respiratory droplets and droplet-nuclei. J. Hyg. (Lond.), 44 (6), 471–4799. doi:10.1017/s0022172400019288

Feng, Y., Marchal, T., Sperry, T., Yi, H. (2020). Influence of wind and relative humidity on the social distancing effectiveness to prevent COVID-19 airborne transmission: A numerical study, J. Aerosol Sci. 147, Article 105585. doi:10.1016/j.jaerosci.2020.105585

Fischer, H., Polikarpov, I., Craievich, A.F. (2004). Average protein density is a molecular-weight-dependent function. Protein Science, 13, 2825–2828. doi:10.1110/ps.04688204

Giovanni, A., Radulesco, T., ĄBouchet, G., Mattei, A., Revis, J., Bogdanski, E., Michel, J. (2020). Transmission of droplet-conveyed infectious agents such as SARS-CoV-2 by speech and vocal exercises during speech therapy: preliminary experiment concerning airflow velocity. Eur. Arch. Otorhinolaryngol., July 16, 1–6. doi:10.1007/s00405-020-06200-7

Jakubczyk, D., Kolwas, M., Derkachov, G., Kolwas, K., Zientara, M. (2012). Evaporation of micro-droplets: the radius-square-law revisited. Acta Physica Polonica, 122, 709–716. doi:10.12693/APhysPolA.122.709

Jayaweera, M., Perera, H., Gunawardana, B., Manatunge, J. (2020). Transmission of COVID-19 virus by droplets and aerosols: A critical review on the unresolved dichotomy. Environ. Res., 188, Article 109819. doi:10.1016/j.envres.2020.109819

Kayser, R., Jr., Bennett, H.S. (1997). Evaporation of a liquid droplet. J. Res. Natl. Bur. Stand. – A Phys. Chem., 81A (2,3), 257–266. doi:10.6028/jres.081A.015

Khan, A.R., Richardson, J.F. (1987). The resistance to motion of a solid sphere in a fluid. Chem. Engin. Commun., 62 (1-6), 135–150. doi:10.1080/00986448708912056

Kukkonen, J., Vesala, T., Kulmala, M. (1989). The interdependence of evaporation and settling for airborne freely falling droplets. J. Aerosol Sci., 20, 749–763. doi:10.1016/0021-8502(89)90087-6

Lapple, C.E. (1951). Particle Dynamics. Eng. Res. Lab., E.I. Du Pont De Nemours and Co., Wilmington, Delaware.

Li, H., Leong, F.Y., Xu, G., Kang, C.W., Lim, K.H., Tan, B.H., Loo, C.M. (2021). Airborne dispersion of droplets during coughing: a physical model of viral transmission. Sci. Rep., 11, Article 4617. doi:10.1038/s41598-021-84245-2

Li, X., Shang, Y., Yan, Y., Yang, L., Tu, J (2018). Modelling of evaporation of cough droplets in inhomogeneous humidity fields using the multi-component Eulerian–Lagrangian approach. Build. Environ., 128, 68–76. doi:10.1016/j.buildenv.2017.11.025

Lieber, C., Melekidis, S., Koch, R., Bauer, H. J. (2021). Insights into the evaporation characteristics of saliva droplets and aerosols: Levitation experiments and numerical modeling. J. Aerosol Sci., 154, Article 105760. doi.org/10.1016/j.jaerosci.2021.105760

Liu, F., Qian, H., Zheng, X., Song, J., Cao, G., Liu, Z. (2019). Evaporation and dispersion of exhaled droplets in stratified environment. IOP Conf. Ser. Mater. Sci. Eng., 609, Article 042059. doi:10.1088/1757-899X/609/4/042059

Liu, S., Novoselac, A. (2014). Transport of airborne particles from an unobstructed cough jet. Aerosol Sci. Technol., 48, 1183–1194. doi:10.1080/02786826.2014.968655

Morawska, L. (2006). Droplet fate in indoor environments, or can we prevent the spread of infection. Indoor Air, 16 (5), 335–347. doi:10.1111/j.1600-0668.2006.00432.x

Morawska, L., Johnson, G.R., Ristovski, Z.D., Hargreaves, M., Mengersen, K., Corbett, S., Chao, C.Y.H., Li, Y., Katoshevski, D. (2009). Size distribution and sites of origin of droplets expelled from the human respiratory tract during expiratory activities. J. Aerosol Sci., 40 (3), 256–269. doi:10.1016/j.jaerosci.2008.11.002

Mittal, R., Meneveau, C., Wu, W. (2020), A mathematical framework for estimating risk of airborne transmission of COVID-19 with application to face mask use and social distancing. Phys. Fluids, 32, Article 101903. doi:10.1063/5.0025476

Netz, R.R. (2020). Mechanisms of airborne infection via evaporating and sedimenting droplets produced by speaking. J. Phys. Chem. B, 124, 7093–7101. doi:10.1021/acs.jpcb.0c05229

Papineni, R.S., Rosenthal, F.S. (1997). The size distribution of droplets in the exhaled breath of healthy human subjects. J. Aerosol Medicine, 10, 105–116. doi:10.1089/jam.1997.10.105

Sarkar, A., Xu, F., Lee, S. (2019). Human saliva and model saliva at bulk to adsorbed phases - similarities and differences. Adv. Colloid Interface Sci., 273, Article 102034. doi:10.1016/j.cis.2019.102034

Schlichting, H. (1979). Boundary Layer Theory, 7th ed. McGraw-Hill, New York.

Stadnytskyi, V., Bax, C.E., Bax, A., Anfinrud, P. (2020). The airborne lifetime of small speech droplets and their potential importance in SARS-CoV-2 transmission. PNAS, 117 (22, 11875–11877. doi:10.1073/pnas.2006874117

Su, Y.-Y., Miles, R.E.H., Li, Z.-M., Reid, J.P., Xu, J. (2018). The evaporation kinetics of pure water droplets at varying drying rates and the use of evaporation rates to infer the gas phase relative humidity. Phys. Chem. Chem. Phys., 20, 23453–23466l. doi:10.1039/C8CP05250F

Sun, W., Ji, J. (2007). Transport of droplets expelled by coughing in ventilated rooms. Indoor Built Environ., 16 (6), 493–504. doi:10.1177/1420326X07084290

Tellier, R., Li, Y., Cowling, B.J., Tang, J.W. (2019). Recognition of aerosol transmission of infectious agents: a commentary. BMC Infect. Dis., 19, 101–109. doi:10.1186/s12879-019-3707-y

Vuorinen, V., et al. (2020). Modelling aerosol transport and virus exposure with numerical simulations in relation to SARS-CoV-2 transmission by inhalation indoors. Safety Science, 130, Article 104866. doi:10.1016/j.ssci.2020.104866

Wang, H., Li, Z., Zhang, X., Zhu, L., Liu, Y., Wang, S. (2020). The motion of respiratory droplets produced by coughing. Phys. Fluids, 32, Article 125102. doi: 10.1063/5.0033849

Wang, Y., Wu, S.H., Yang, Y., Yang, X.N., Song, H., Cao, Z.X., Huang, Y.Q. (2019). Evaporation and movement of fine droplets in non-uniform temperature and humidity field. Build. Environ., 150, 75–87. doi:10.1016/j.buildenv.2019.01.003

Wells, W.F. (1934). On air-borne infection study II: droplets and droplet nuclei. Am. J. Hyg., 20, 611–618. doi:10.1093/oxfordjournals.aje.a118097

White, F.M. (2006). Viscous Fluid Flow, 3rd ed. McGraw-Hill, New York.

Xie, X., Li, Y., Chwang, A.T.Y., Ho, P.L., Seto, W.H. (2007). How far droplets can move in indoor environments - revisiting the Wells evaporation-falling curve. Indoor Air 17, 211–225. doi:10.1111/j.1600-0668.2007.00469

Xie, X., Li, Y., Sun, H., Liu, L. (2009). Exhaled droplets due to talking and coughing. J. R. Soc. Interface, 6, S703–S714. doi:10.1098/rsif.2009.0388.focus

Zhu, S., Kato, S., Yang, J.-H. (2006). Study on transport characteristics of saliva droplets produced by coughing in a calm indoor environment. Build. Environ., 41, 1691–1702. doi:10.1016/j.buildenv.2005.06.024

Марко В. Лубарда, Владо А. Лубарда

О кретању испаравајуће респираторне капљице

С а ж е т а к

У раду је дата анализа кретања испаравајуће респираторне капљице емитоване говором, кашљањем или кијањем. Отпор ваздуха је представљен нелинеарном функцијом брзине капљице, а брзина смањења површине омотача капљице функцијом релативне влажности и температуре ваздуха. Претпостављени почетни тежински садржај капљице је 98% вода, 1% NaCl и 1% протеин. Пораст густине капљице током њеног кретања и испаравања је одређен до тренутка када капљица испари до свог језгра (резидуума) које се састоји од соли и протеина. Нумеричко рјешење диференцијалних једначина дефинише путању капљице различите почетне величине и брзине емитовања, при различитим вриједностима релативне влажности и брзине испаравања. Максималне хоризонталне и вертикалне дистанце које капљице досегну су срачунате у одсуству и присуству струјања ваздуха. Резултати су анализирани у контексту ризика од ширења вируса капљичним путем.

Кључне ријечи: брзина испаравања; густина; капљично језгро; сила отпора; релативна влажност; респираторна капљица; SARS-CoV-2; утицај вјетра